Thermochimica Acta, 58 (1982) 211–229
Elsevier Scientific Publishing Company, Amsterdam—Printed in The Netherlands

EFFECT OF AUTOCLAVING ON ZINC OXIDE IN THE PRESENCE OF SULPHATE IONS

SUZY A. SELIM

Chemistry Department, Faculty of Science, Ain Shams University, Cairo (Egypt)

ANWAR AMIN

Chemistry Department, Faculty of Education, Ain Shams University, Cairo (Egypt)

PAUL G. ROUXHET

Université Catholique de Louvain, Groupe de Physico-Chimie Minérale et de Catalyse, B-1348 Louvain-La-Neuve (Belgium)

(Received 23 March 1982)

ABSTRACT

The effect of autoclaving a zinc oxide preparation containing SO_4^{2-} under 5 and 10 atmospheres is studied by combining X-ray diffraction, differential thermal analysis, thermogravimetry and IR spectroscopy. Textural measurements are also carried out on the parent samples and those produced in the temperature range 200–1000°C.

A new phase of a basic carbonate–sulphate, including ammonia in its coordination shell, is observed in the original preparation and having its *d* distances at 11.060, 8.954 and 2.714 Å. This is transformed to another phase at ~180°C which is also the main phase characterizing the autoclaved samples, and belongs to a basic zinc oxide–sulphate possessing *d* distances at 7.055, 2.468 and 2.805 Å. Autoclaving the oxide preparation under 10 atm gives hexagonal zinc oxide of high purity and crystallinity at 1000°C. An empirical formula is given for the oxide preparation which describes the different decomposition stages observed. At ~390°C, a reversible reduction process comprising oxygen evolution is observed.

Autoclaving increases the area of the parent oxide and at temperatures below 600°C is a function of the structural changes. The autoclaving pressure is insignificant ⩾600°C.

Pore structure analysis showed all the samples to be predominantly mesoporous, coexisting with some micropores except that autoclaved under 5 atm and heated at 250°C which is predominantly microporous. Autoclaving under 5 atm causes narrowing of the pores for products below 600°C. Autoclaving has little effect on the average pore radius ⩾600°C.

Evaluation of the average pore radius from the constructed *t*-curves for parallel-plate pore idealization is discussed.

0040-6031/82/0000–0000/$02.75

INTRODUCTION

The non-stoichiometry present in zinc oxide and its departure in the metal-rich direction make it important as a catalyst, in chemical industries, and as a photoconductor. The high activity of zinc oxide lies in its ability to cause dissociative adsorption on a number of ZnO pair sites for chemisorbed molecules such as water [1], hydrogen [2], ammonia and carbon dioxide [3]. Several studies on the adsorption of water [4–6] and its reversibility [7] are attempted but much of the peculiarities of this oxide still remain obscure.

The addition of additives [8,9] and pretreatment of oxides are known to vary the catalytic, acidic and basic properties [10,11] as well as the surface texture [12,13]. In particular the presence of small amounts of SO_4^{2-} ions is found to increase both the acidity and acid strength [14], whereas increased amounts are useful for the manufacture of oriented ZnO [15]. The effect of autoclaving zinc oxide in the presence of such an anion is then of great value in further clarifying the nature of such a modified catalyst and this is the goal of the present investigation. A systematic structural and textural study is given using such techniques as XRD, DTA, TG, IR spectroscopy and low temperature adsorption of nitrogen.

EXPERIMENTAL

Zinc oxide (Z) is prepared by flushing from a douche a solution of 1 M ammonia into a well stirred solution of 1 M $ZnSO_4$ (Mallinchrodt, U.S.A.) at room temperature. The precipitate is washed twice with 1% ammonia solution to keep some sulphate in the solid [15], and dried to constant weight at room temperature in the presence of an air current. Chemical and TG analysis showed that the solid contains 16.55% SO_4^{2-} and 48.62% Zn. Two batches of this precipitate are autoclaved under 5 atm (ZI) at a temperature of $\sim 121°C$, and under 10 atm (ZII), the temperature reaching $\sim 180°C$, each for 5 h. Dehydration products are obtained for the above samples by heating in the temperature range 250–1000°C for 2 h in the presence of air. The treatment temperature will always follow the preparation symbol.

TG analysis is carried out in the presence of static air using a Stanton-Redcroft thermobalance Type 750/770 connected to a BD 9 two-channel automatic recorder 'Kipp and Zonnen' at a heating rate of 5°C min^{-1}. In the differential thermal analysis experiments, α-alumina is used as inert standard and a programme temperature controller 'Ether' transitrol type 994/2 permits a linear heating rate of 12°C min^{-1}, and a Cambridge Recorder Model 'B' is used for recording the temperature difference.

XRD patterns are recorded by a Philips diffraction unit using Ni-filtered Cu K_α radiation.

The cell used to measure the IR spectra of adsorbed pyridine (Merck) has been described earlier [16]. The absorption spectra are measured with a Perkin-Elmer 180 spectrograph flushed with dry nitrogen. IR spectra for the bulk of the samples are measured with a Pye-Unicam SP3-200A spectrograph using KBr pellets.

Adsorption–desorption isotherms of nitrogen at 77 K are determined by conventional volumetric gas adsorption.

RESULTS AND DISCUSSION

Structural characterization

Chemical analysis indicates the presence of ammonia and carbonate in preparation Z; the latter being formed [5] during the preparation by atmospheric carbon dioxide, probably through its dissolution.

The X-ray diffraction pattern of the original sample (Z) points to the presence of zinc hydroxide together with a main characteristic band at a *d* distance of 11.06 Å and the bands at 8.954 Å and 2.714 Å which do not characterize any possible structure of a zinc compound [17] that could possibly form in the presence of the prevailing ions during the preparation (Fig. 1). The hydroxide pattern is no longer observed at 100°C and the remaining crystalline phase is better defined. Heating at 120°C does not affect the phase present, whereas at 180°C a new phase is observed in the 2θ range of 11–13 Å with the main characteristic band at a *d* distance of 7.31 Å. The remaining bands, which are of lower intensities, are those characterizing the decomposing phase.

Zinc oxide commences to form at 220°C, and at 400°C the hexagonal ZnO structure is well established besides the formation of compounds of different oxide: sulphate ratio, namely that of $Zn_3O(SO_4)$ and $Zn_5O_2(SO_4)_3$ [17]. At 1000°C, hexagonal ZnO is obtained with the appearance of two very small bands at 2θ values of 5.575 Å and 3.740 Å which may be characteristic of traces of $Zn(S_2O_4)$ [17] formed during the decomposition of the sulphate.

TG analysis of this sample shows two clear steps terminating at ~100°C and 120°C followed by a large step covering the temperature range 120–420°C, together with a very small but persisting step in the range 400–420°C (Fig. 2). Above 750°C, the large step observed is responsible for the decomposition of the sulphate in the sample.

The DTA curve of this sample exhibits endothermic effects at ~95, ~115, ~185, ~210 and ~245°C and a smaller one at 370°C (Fig. 3).

IR spectra of sample Z and Z-120 are identical and show the same characteristic carbonate vibrational bands as those produced by a carbonate preparation made by using Na_2CO_3 and $ZnSO_4$ at room temperature (Fig. 4). Characteristic vibrational bands are observed at 1502, 1392, 832 and 706 cm^{-1} typical of the ν_3, ν_1, ν_2 and ν_4 vibrations [18]. It should be noted that the XRD of samples Z and Z-120 did not show the characteristic bands of

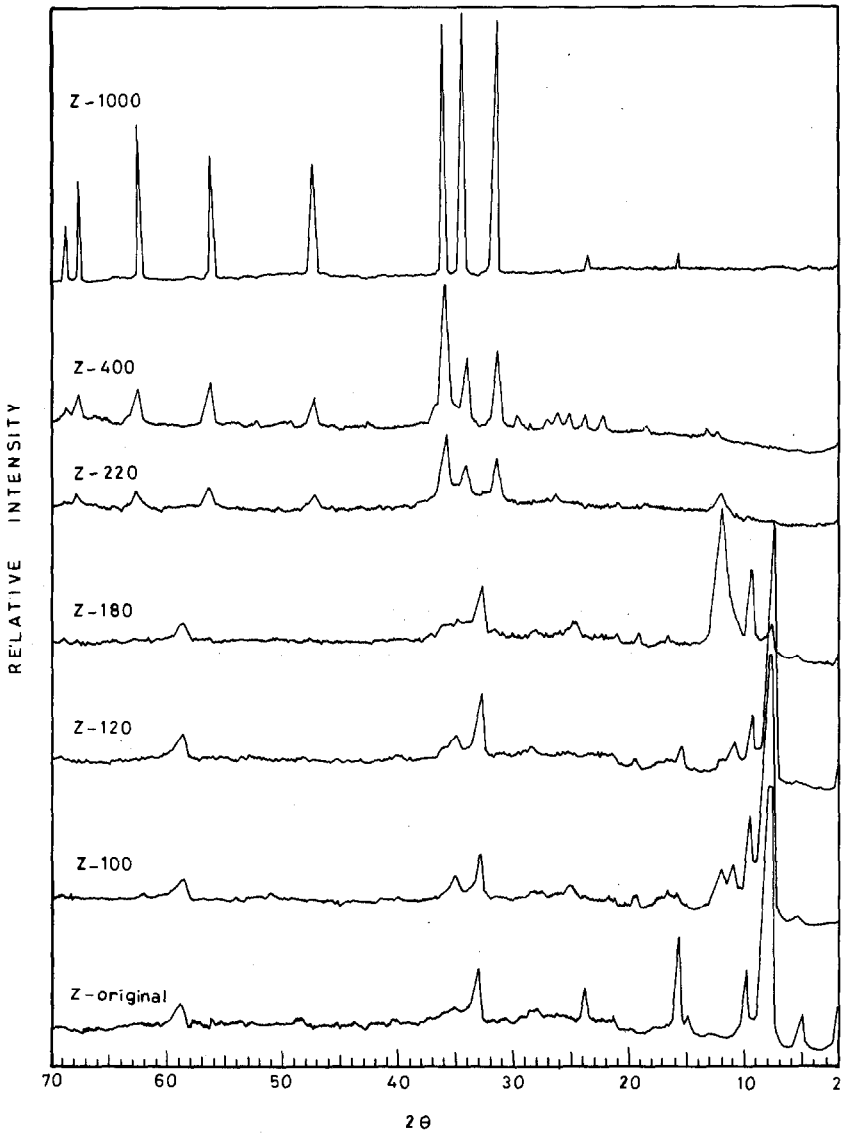

Fig. 1. X-Ray diffraction patterns of sample Z and its thermally treated products.

$ZnCO_3$. The ν_1 vibration which is normally forbidden in the free carbonate ion, becomes IR active for unidentate and bidentate carbonato complexes. A comparison with published data [18] shows that in the present sample the metal is directly attached to one oxygen, i.e. it forms a unidentate compound

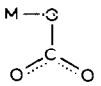

and therefore a complex seems to be formed containing the carbonate and sulphate anions together.

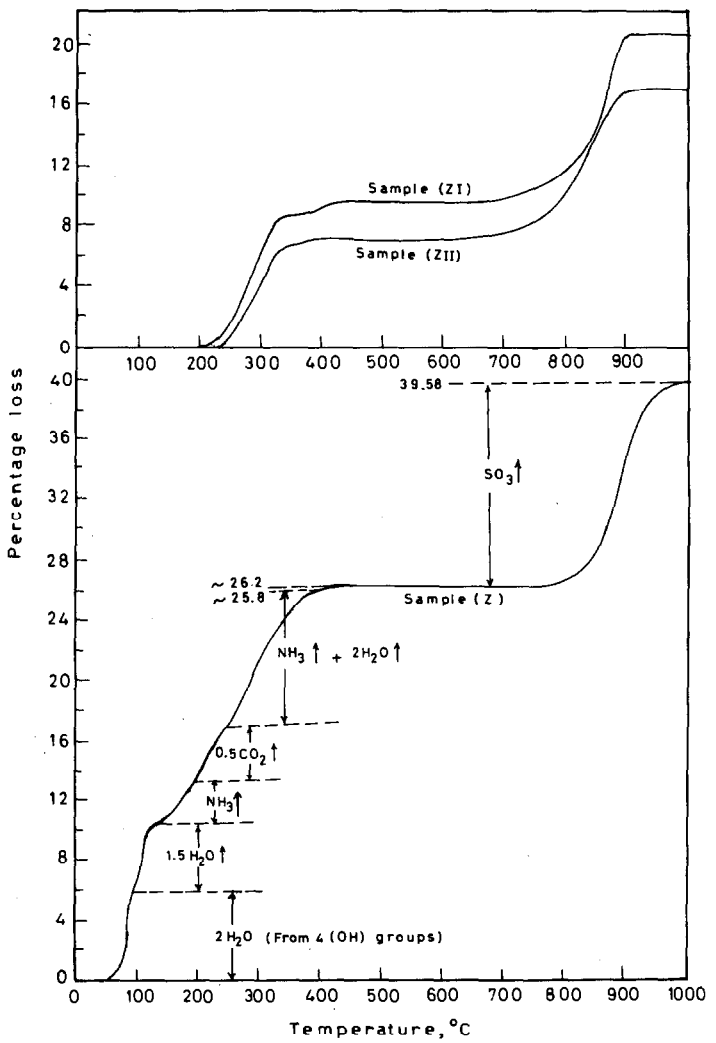

Fig. 2. Thermogravimetric curves for sample Z and the autoclaved samples ZI and ZII.

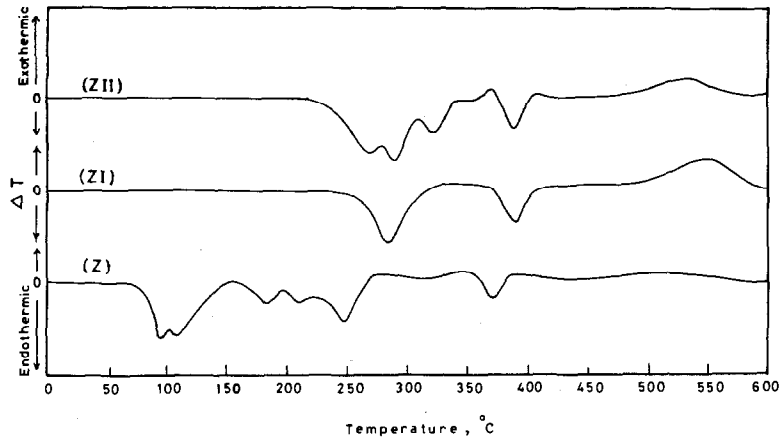

Fig. 3. Differential thermal analysis curves of the unautoclaved sample Z and the autoclaved samples ZI and ZII.

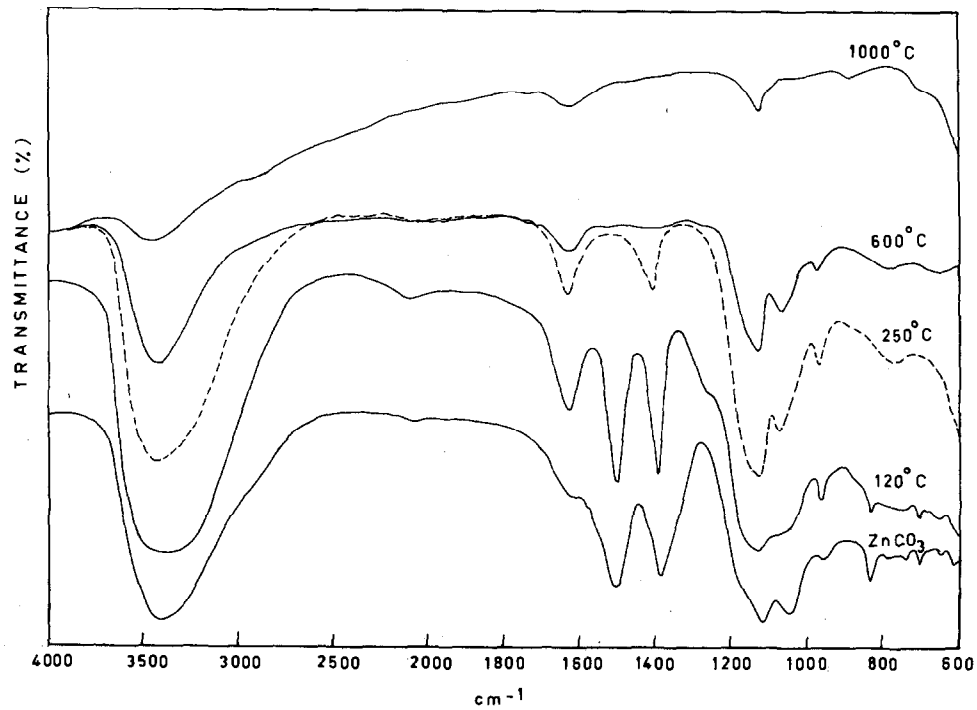

Fig. 4. Bulk IR spectra of $ZnCO_3$ and sample Z treated at various temperatures.

The band at 1392 cm^{-1} is found to be reinforced by the presence of ammonia, traces of which were still present in sample Z-250. The H–N–H deformation vibrational band characteristic for the NH_4^+ ion appears at ~ 1400 cm^{-1} [19]. N–H stretching vibrational bands are also observed in the region 3200–3350 cm^{-1}, overlapping with those for the O–H stretching vibrations. Disproportionation of ammonia [20] and water [1] by chemisorption on ZnO is known to take place.

From the above data, the endotherms at ~ 95°C and ~ 115°C result from the decomposition of the hydroxide present and from the evolution of the adsorbed water, respectively. These processes give rise to the first two steps observed in the TG curve (Fig. 2). No ammonia is evolved in this temperature range. The small step observed in the temperature range 150–180°C (Fig. 2) and giving rise to the endotherm at 185°C may arise from the evolution of either a water or an ammonia molecule. By comparison with the results obtained for the autoclaved samples, and discussed later, it appears that it is the ammonia which is evolved. This is found to affect the crystal structure, as reflected in the variation observed in the 2θ range of 8°–12.5°. It is to be recalled that differences in the temperature of any particular process as observed from TG and DTA arise from the different transfer processes in the two techniques.

The XRD pattern of sample Z-180 shows that the prevailing phase, called for convenience a 'basic carbonate sulphate' complex, is decomposing. Carbon dioxide, ammonia and water are evolved upon decomposition, giving rise to the endotherms at 210°C for CO_2 and 245°C for water and ammonia, and also for the corresponding steps observed in the TG curve.

The observed endotherm at ~ 370°C (Fig. 3) is believed to result from the evolution of oxygen from the solid material, leaving behind a non-stoichiometric oxide. The weight loss observed at ~ 400°C in the TG curve is quite small to result from water evolution and is found to be completely reversible. Thus if the heating is conducted up to ~ 500°C, followed by cooling, the step is immediately reproduced in the cooling curve as a weight gain. The appearance of this step in the DTA and TG curves of the autoclaved samples, which possess a different structure than sample (Z) (Figs. 6 and 1, respectively), favours the belief that it is oxygen that is evolved and not water. It is worth noting that if samples heated up to 500°C are cooled overnight, their TG curves also show two major steps arising from the surface adsorption of CO_2 and H_2O from the atmosphere [1] but which do not seem to form any carbonate in the sample, as concluded from their corresponding bulk IR spectra and XRD patterns.

Decomposition of the sulphate commences at 800°C to produce hexagonal ZnO. An empirical formula is suggested for this zinc oxide preparation, viz. $\{Zn_{4.5}O(OH)_4(NH_3)_2(H_2O)_2(CO_3)_{0.5}SO_4\}1.5\ H_2O$, which gives concor-

dant results with the different decomposition stages according to their corresponding weight losses as presented in Fig. 2.

Chemical and IR spectral analysis of autoclaved sample ZII show it to be ammonia-free, whereas sample ZI contains traces of ammonia. Both samples are free from any carbonate compounds (Fig. 5) and autoclaving seems to have hydrolyzed the carbonate originally present in preparation (Z). However, both samples adsorb some atmospheric CO_2 to a small extent.

XRD patterns of ZI and ZII are nearly similar. That of ZI exhibits its most intense band at a *d* distance of 7.140 Å which is slightly shifted to 7.055 Å for sample ZII. The characteristic bands for hexagonal zinc oxide are relatively intense in both patterns, being greater for sample ZII than for sample ZI, together with the presence of some weaker bands characterizing $ZnSO_4 \cdot n\ H_2O$, where *n* varies below one for both samples. The characteristic oxide pattern increases at 250°C and is accompanied by a corresponding decrease in those identifying the zinc sulphate and the band at a *d* distance in the range 7.055–7.140 Å.

At 1000°C, sample ZI retains a reduced band at a *d* distance of 7.14 Å with the well-defined hexagonal zinc oxide, whereas sample ZII exhibits the pattern of the pure oxide. Thus autoclaving under 10 atm facilitates the production of pure hexagonal zinc oxide. Typical XRD patterns for sample ZI and its products obtained at 250 and 1000°C are shown in Fig. 6.

The appearance of the main band at the *d* distance of 7.055 and 7.140 Å for autoclaved samples ZII and ZI, respectively, together with those characteristic for the oxide, below ~250°C, suggests the presence of a basic zinc

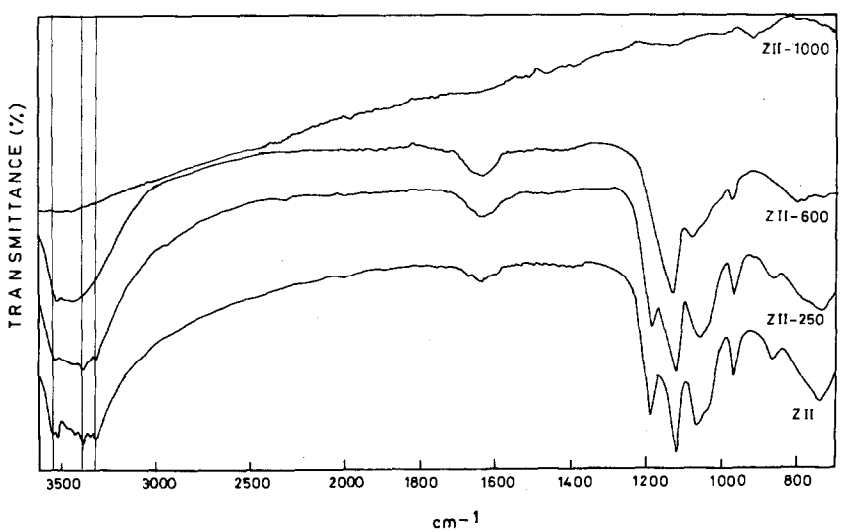

Fig. 5. Bulk IR spectra of ZII and its products obtained at different temperatures.

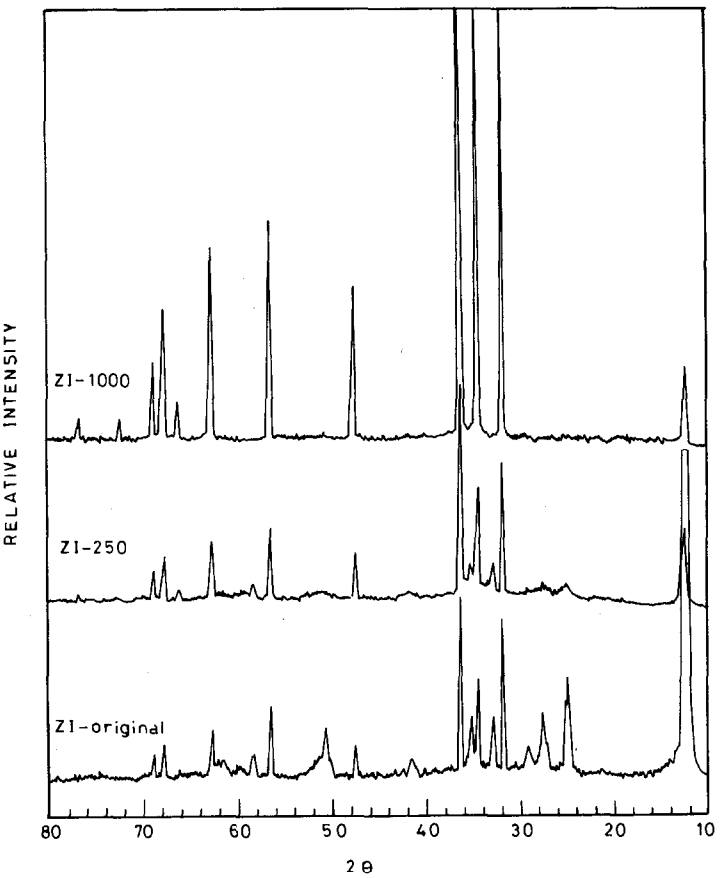

Fig. 6. X-Ray diffraction patterns for sample ZI and its products obtained at 250 and 1000°C.

oxide–sulphate phase with characteristic *d* distances of 7.055, 2.468 and 2.805, as found for ZII. This structure appears to be stable, being still present for sample ZI heated at 1000°C.

Both samples ZI and ZII are unaffected by thermal treatment below 200°C, the samples behaving passively towards the adsorption of atmospheric water vapour (Fig. 2). The TG curve of ZI shows one large step which terminates at ~350°C followed by a very small step at ~420°C which is slightly bigger than that observed for sample Z. Corresponding endotherms are observed at 285 and 390°C (Fig. 3). The large step observed in the TG curve of ZI is split into two main steps for sample ZII. The first, terminating at ~300°C, is responsible for the endotherms at 270 and 290°C. The second, terminating at 370°C, is accompanied by the endotherm at 325°C. The small step at ~390°C is similar to that observed for ZI and Z

which also reproduces the corresponding endotherm at 390°C and is responsible for the evolution of some oxygen, as previously mentioned for sample Z.

It is of significance to note that if the autoclaved samples are heated to about 400°C they lose their passiveness towards adsorption of atmospheric water vapour. Thus after cooling overnight, their TG curves exhibit the loss of physically adsorbed water at about 115°C. Hence, autoclaving preparation (Z) under 5 or 10 atm affects the surface in such a way as to neutralize any surface residual fields of force whereby no further attraction to the atmospheric water vapour could take place. Thermal treatment of these autoclaved samples causes the loss of this passiveness.

Bulk IR spectra of sample ZII show four defined O–H stretching vibrational bands at 3308, 3380, 3530 and 3620 cm^{-1}. The last one belongs to a least stable hydroxyl, disappearing from sample ZII-250. They may be situated at adjacent sites at or near the surface [1] and are probably responsible for the endotherm at 270°C. The two other endotherms at 290 and 325°C correspond to the dehydroxylation of the remaining hydroxyl groups. It is difficult at this stage to assign the remaining O–H vibrations with the corresponding endotherms due to an overlap of the latter.

Heating both unautoclaved and autoclaved zinc oxide to 600°C, where dehydroxylation is virtually complete, followed by exposure to the atmosphere, is found to rehydroxylate, exhibiting a broad band centred at 3450 and a narrow one at 3520 cm^{-1} which represent two easily hydroxylated sites in the zinc oxide samples. However, when the heating is conducted to 1000°C only samples from Z and ZI show the band centred at 3450 but with a much reduced intensity together with a small band at 1120 cm^{-1} which may be due to the M–O–H bending mode [18]; that at 3520 disappeared. No bands are observed for sample ZII-1000 which is treated under high water vapour pressure. Such a treatment seems to have an active role in producing a pure and well-ordered crystal structure besides being inactive towards hydroxylation by atmospheric water vapour.

Autoclaving is found to decrease the decomposition temperature of the sulphate present in the samples, being ~ 750 and ~ 700°C for samples ZI and ZII, respectively, compared to 800°C for sample Z. It is also found to hydrolyze a fraction of the sulphate present, as found by both chemical and TG analysis; the sulphate concentration being 16.55%, 13.92% and 11.76% for samples Z, ZI and ZII, respectively.

Surface IR spectroscopy of sample Z heated at 500°C in vacuo shows the complete absence of any hydroxyl groups. Adsorption of pyridine on this sample indicates the presence of Lewis acid sites only as previously reported [21]. Outgassing at 150°C for 2 h does not remove all the pyridine from the solid surface.

Surface area and pore structure

The N_2 adsorption–desorption isotherms are obtained at −196°C for sample Z, the autoclaved samples ZI and ZII and their thermally treated products. The adsorption isotherms of all the samples are type II, except those obtained for samples ZI-1000, ZII and ZII-1000 which are near type III and show an initial linear region which extends to intermediate relative pressures.

Isotherms of samples Z, ZI and their thermally treated products, except Z-250, Z-500, ZI-400 and ZI-500, exhibit closed hysteresis loops as well as those of sample ZII and its thermally treated products up to 600°C. The shapes of the hysteresis loops indicate a wide variation of pore size. The rest of the isotherms are completely reversible.

The nitrogen surface areas, S_{BET}, are obtained by using the Brunauer–Emmett–Teller (BET) equation, assuming that the nitrogen molecule occupies an average area of 16.2 $Å^2$ in the complete monolayer. In the case of samples of near type III and possessing a BET c-constant of about 3, the area is obtained for the sake of comparison with the other samples (yet not reliable) by assuming an approximate value for C and locating $(P/P_0)_m$ from which the monolayer capacity is obtained [22]. The samples are generally characterized by low BET c-constants, except sample ZI-250 which is high, being 131 (Tables 1 and 2).

The specific surface area of the unautoclaved sample Z increased upon thermal treatment to 400°C (Fig. 7). The evolution of ammonia, CO_2 and water vapour below this temperature creates new pores and channels whereby the area is increased. During this process some of the evolved vapours become adsorbed and the growth of the adsorbed layer may lead to pore blocking of the narrower pores. The size of the pores may become of such dimension that no capillary condensation occurs [23], as is the case with sample Z-250 where only multimolecular adsorption takes place. Narrowing of the mesopores is also observed from the data of the average pore radii obtained as $\bar{r}_H = V_{P_{0.95}}/S_{BET}$ (Fig. 7, and Table 1). Above 250°C these adsorbed molecules are evolved, causing widening of the pores that are already present and exposing a new surface of the previously blocked pores. These changes are reflected in the values of total pore volume taken at $P/P_0 = 0.95$ (Table 1). No structural changes occur in the temperature range 400–600°C and a continuous decrease in area is observed. The pore volume decreased markedly at 500°C and shrinkage of the solid matrix is accompanied by pore narrowing hindering the occurrence of capillary condensation. At 600°C, widening of the pore system occurs at the expense of some of the narrower ones, thus increasing the total pore volume. The decomposition of the sulphate–oxide structure above 600°C increases the area drastically where,

TABLE 1

Some surface parameters of unautoclaved zinc oxide, Z, and its thermally treated products

Sample	BET *c*-constant	S_{BET} ($m^2\ g^{-1}$)	S_t ($m^2\ g^{-1}$)	$V_{P_{0.95}}$ ($ml\ g^{-1}$)	$\bar{r}_{H_{0.9}}$ (Å)	$\bar{r}_{H_{0.95}}$ (Å)	$\bar{r}_{H_{1.0}}$ (Å)	$\bar{r}_{H_t}$ (Å)
Z-original	7	124.3	135.0	0.2674	15.6	21.5	44.5	26.6
Z-250	6	179.7	188.0	0.2440	12.3	13.6	16.4	15.4
Z-400	7	230.1	232.0	0.4663	15.9	20.3	27.0	23.6
Z-500	4	167.3	158.0	0.2238	11.5	13.4	28.8	12.4
Z-600	6	142.6	147.0	0.2518	12.9	17.7	32.7	13.0
Z-1000	4	518.0	495.0	0.6063	9.6	11.7	17.1	12.0

TABLE 2

Some surface parameters of the autoclaved zinc oxide ZI, ZII and their thermally treated products

Treatment temperature (°C)	Sample ZI					Sample ZII				
	BET *c*-constant	S_{BET} ($m^2\ g^{-1}$)	S_t ($m^2\ g^{-1}$)	$V_{P_{0.95}}$ ($ml\ g^{-1}$)	$\bar{r}_{H_t}$ (Å)	BET *c*-constant	S_{BET} ($m^2\ g^{-1}$)	S_t ($m^2\ g^{-1}$)	$V_{P_{0.95}}$ ($ml\ g^{-1}$)	$\bar{r}_{H_t}$ (Å)
Original	5	277.0	290.0	0.4477	14.0	3	237.5 [a]	-	0.2891	
250	131	332.0	338.0	0.3016	10.0	4	158.7	159.0	0.2332	13.0
400	6	120.5	123.0	0.1865	14.6	14	101.1	108.0	0.2130	26.0
500	5	260.5	260.0	0.3140		7	75.0	73.0	0.1243	19.0
600	11	93.9	99.0	0.1819	18.0	6	94.9	95.0	0.1601	23.0
1000	3	324.6 [a]		0.3575		3	322.2 [a]		0.3218	

[a] Areas obtained for the sake of comparison [22].

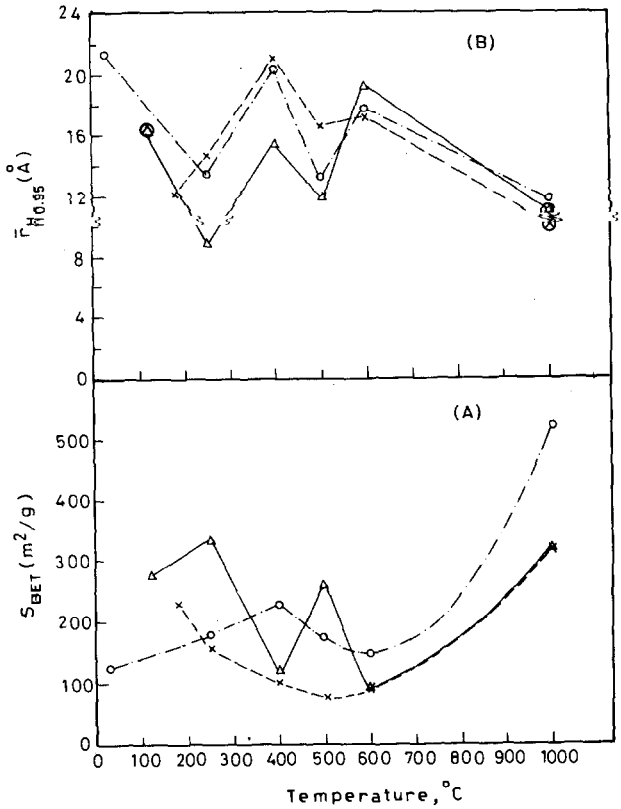

Fig. 7. Variation of (A) specific surface area, S_{BET}, and (B) average pore radius, $\bar{r}_{H_{0.95}}$, with treatment temperature for samples Z (○), ZI (△) and ZII (×). Encircled values are obtained for comparison only.

at 1000°C, the area of zinc oxide is about four times that of the original preparation, accompanied by the creation of narrow pores and a large increase in total pore volume. A similar observation of increasing the area of the oxide by anion additions has been observed in other oxide systems [14,24].

Differences in the autoclaving pressure give rise to different trends in area variation below 600°C resulting from small differences in their decomposition stages. Thus autoclaving sample Z under 5 atm (~ 121°C) increases the area markedly and gives rise to a much narrower pore system with $\bar{r}_H \approx 16$ Å (Fig. 7B). The rate of evolution of the different decomposition products (H_2O, NH_3, CO_2) at ~ 121°C is decreased by the presence of the water vapour of the autoclave, giving them sufficient time to diffuse out of the narrower pores thereby hindering their blocking. This is also reflected by the low closure pressure of the hysteresis loop ($P/P_0 \sim 0.2$). The total pore volume $V_{P_{0.95}}$ is expected to be high (Table 2). The evolution of the remaining

ammonia from sample ZI by heating up to 250°C further increases the area and during this process narrow pores are created at the expense of the wider pores, therefore decreasing $V_{P_{0.95}}$. DTA shows an endotherm at 285°C, whereas TG analysis shows a relatively increased weight loss at ~420°C (Fig. 2). Some of the water pre-evolved at the lower temperatures has been adsorbed on the surface (see previous section). The desorption of these gases together with the stabilization of prevailing crystalline phase causes some shrinkage of the solid matrix whereby the narrower pores become inaccessible to the nitrogen molecules, resulting in a decrease in pore volume (Table 2) and an increase in average pore radius (Fig. 7B). During this process, some of the adsorbed vapours are trapped but are then evolved above 400°C, giving rise to the observed increase in area at 500°C and the increased loss in the TG step at 420°C over that necessary for the partial reduction process taking place at this temperature. The appearance of a fraction of narrower pores is thus excepted together with an increase in $V_{P_{0.95}}$. Sintering of the solid material is observed at 600°C and a decrease in both the area and $V_{P_{0.95}}$ is accompanied by pore widening.

Sample ZII, on the other hand, shows a continuous decrease in area up to 500°C but the changes brought about in the pore system varied with temperature (Fig. 7). No ammonia is detected in sample ZII and the evolution of the water vapour up to 400°C causes widening of the pore system (Fig. 7B) at the expense of the narrower ones, thereby decreasing $V_{P_{0.95}}$ (Table 2). At 500°C, pore narrowing is revealed not only by $\bar{r}_{H_{0.95}}$ or $V_{P_{0.95}}$ values but also by the complete reversibility of the adsorption isotherm. The decomposition of the sulphate appears to be initiated by heating at 600°C (Fig. 2) and the area is slightly increased as well as $\bar{r}_{H_{0.95}}$ and $V_{P_{0.95}}$.

Similar to sample Z, above 600°C the area greatly increases for both autoclaved samples due to the complete decomposition to the oxide and is almost the same for them both, being 324.6 and 322.2 $m^2\ g^{-1}$, respectively. The total pore volume of both samples also increases (Table 2) resulting from the increase in the narrow pores formed. The $\bar{r}_{H_{0.95}}$ values of samples ZII, ZI-1000 and ZII-1000 are evaluated for the sake of an approximate comparison with the rest of the data but should be considered with caution as their corresponding S_{BET} values are not so reliable.

The modification of the surface texture is also observed by carrying out a pore structure analysis using De Boer's *t*-method [25]. The *t*-curves used in these plots are those of Mikhail et al. [26] (BET *c*-constant < 20), and Sing and co-workers [27] (BET *c*-constant ~ 100) which fulfilled the criteria [28] for their proper choice to compute a correct S_t value which should be comparable with S_{BET}. Agreement between S_t and S_{BET} is observed for all samples with BET *c*-constant ≥ 4. No V_1–*t* plots are obtained for samples with BET *c*-constant below 4.

For sample Z and its product, at 250°C two regions of upward deviations are observed commencing at a thickness of 3 Å and 5.2 Å (Fig. 8). The upward deviations do not continue for both samples and revert back to the original slope at $t = 16.2$ Å and 11 Å, respectively. These two regions of

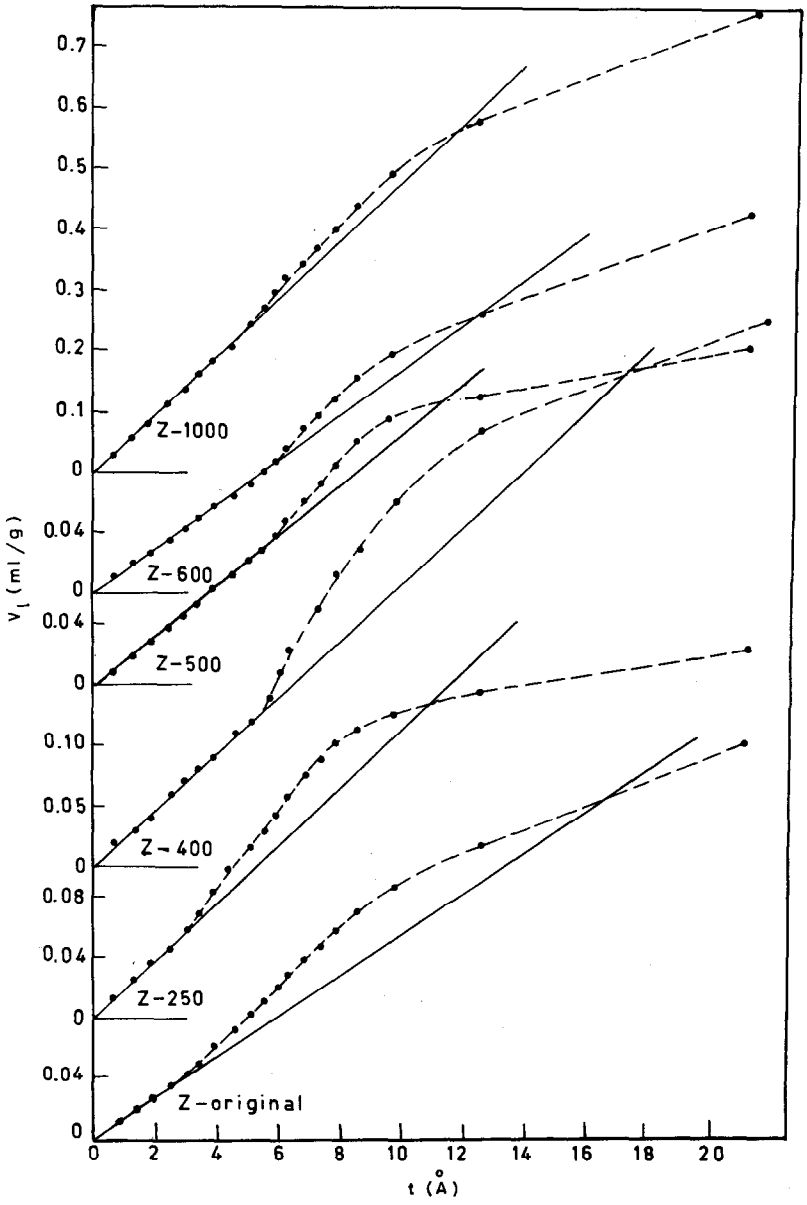

Fig. 8. V_1–t plots of sample (Z) and its thermally treated products.

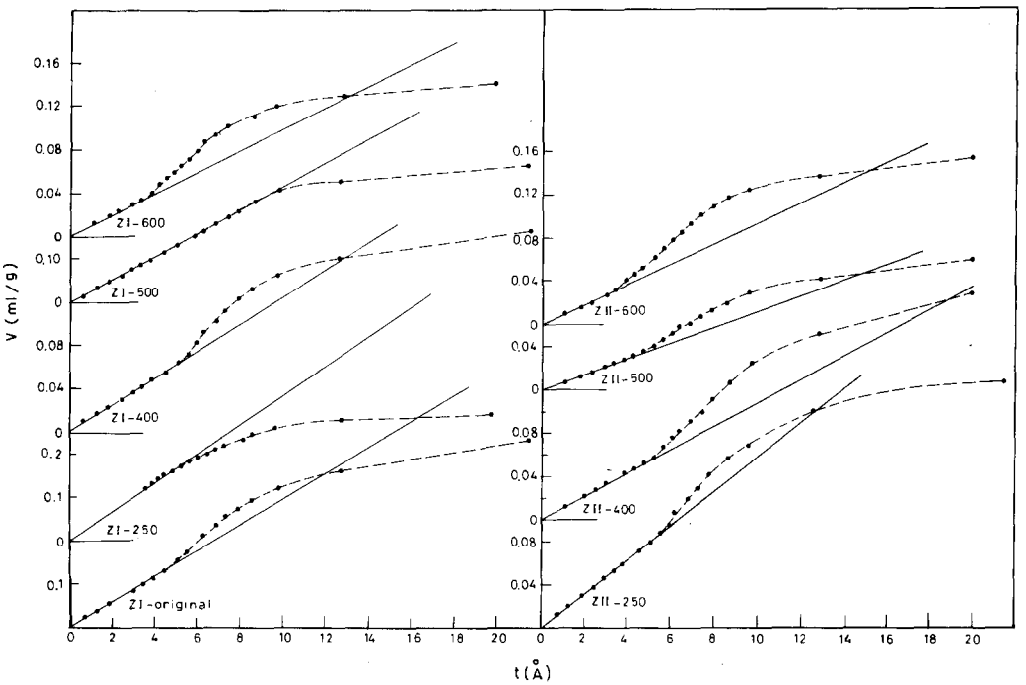

Fig. 9. V_l–t plots of autoclaved sample (ZI) and the thermally treated products of samples (ZI) and (ZII).

upward deviations indicate the presence of two groups of mesopores coexisting with the micropores. Above 250°C only one group of mesopores coexist with the micropores.

Autoclaving sample Z under 5 atm causes narrowing of the pore system and the group of wide pores that appeared at t-values below 5.2 Å for sample Z are absent from this sample though it still constitutes both meso- and micropores (Fig. 9A). Microporosity is exhibited by sample ZI-250 and a downward deviation is observed at $t = 5$ Å. As previously observed for $\bar{r}_{H_{0.95}}$, widening of the pores takes place by heating at 400°C and the upward deviation commences at $t = 5.5$ Å and reverts back at $t = 13$ Å, showing the presence of a mixed pore system. A linear V_l–t plot such as that of ZI-500, which is similar to that produced on the surface of non-porous adsorbents, could be produced by solids with a parallel-plate pore structure whose pore width does not permit capillary condensation to take place. However, this pore narrowing is reflected in the $\bar{r}_{H_{0.95}}$ values (Fig. 7B). Widening of the pores at 600°C is confirmed by the reappearance of the upward deviation commencing at $t = 4$ Å and reverting back at $t = 13$ Å, showing a larger fraction of wide pores than for sample ZI-400.

Autoclaving under 10 atm gives rise to heated products possessing pore structures different to that autoclaved under 5 atms. Thus sample ZH-250 possesses both meso- and micropores, showing an upward deviation at $t = 6$ Å and intersecting back the original slope at $t = 12.5$ Å (Fig. 9B). At 400°C, much widening is observed from the upward deviation and the reverting back takes place at a high t-value of 19.8 Å, in which case mesoporosity predominates. The upward deviations observed in the V_l–t plots of products heated in the temperature range 250–500°C all commence in the t-value range of 5–6 Å. The reverting back of the t-curve of sample ZH-500 at a lower t-value than for ZH-400, namely at $t = 14.5$ Å, shows an increase in microporosity. Further heating to 600°C causes some widening where the commencement of upward deviation occurs at a lower t-value, namely 3.5 Å.

From the various shapes of these t-curves obtained for solids with mixed pore systems and having a parallel-plate pore idealization, it is possible to obtain an average value for $\bar{r}_H$ considered to give a more reliable value than that obtained from the equation V_P/S_{BET} which might suffer errors in the choice of the relative pressure, above 0.9, at which the volume, V_p, is to be taken [29], as well as errors in S_{BET} arising from the molecular area where the packing conditions may vary. The upward deviation of the t-curve of the sample compared to that of the non-porous reference and its reverting back and intersection with the original slope points to an average thickness $(d-t)_{ave.}$ required to completely fill the pores with capillary condensed liquid, where d is the average half distance between the walls of the pores and t is the statistical thickness of the adsorbed layer. Thus subtraction of the thickness corresponding to the reverting back to the original slope from that where an initial upward deviation takes place gives an average of the thickness of this 'condensed' film in the pores, which represents the range of thickness where adsorption exceeds that normally occurring on the non-porous reference. This condensed adsorbate is usually preceded by an already adsorbed layer corresponding to a certain thickness whose value may be either smaller or greater than half that of d, i.e. $t < \text{or} > d/2$, depending on the relative pressure and the size of the pores. If on the average the thickness of this condensed film is considered to be equal to the average of the thickness of the adsorbed layers in the pores, i.e. $(d-t)_{ave.} \approx t_{ave.}$, then multiplying the thickness obtained experimentally for the condensed film by 2 would give a value for the average hydraulic radius denoted by $\bar{r}_{H_t}$. Comparison of the values of $\bar{r}_{H_t}$ obtained from the t-curves of sample Z and its heated products (Table 1) with the average pore radii obtained by employing V_p values taken at P/P_0 ranging from 0.90 to 1.0 (Table 1) shows that in all cases, except Z-500 and Z-600, $\bar{r}_{H_t}$ values are slightly greater than $\bar{r}_{H_{0.95}}$, which shows that identical results could have been produced if V_p is read off at relative pressures slightly greater than 0.95. For samples Z-500

and Z-600 a value of V_p taken between relative pressures 0.90 and 0.95 would give rise to concordant results between the two methods of evaluating the average pore radius. Thus the computation of the average hydraulic radius from the *t*-curves avoids the choice of any parameter at an arbitrary value and thus gives a much reliable estimation for the average pore radius. Table 2 gives the r_{H_t} values for samples ZI and ZII and their heated products which reproduce the same picture of pore size variation upon heat treatment as those of $\bar{r}_{H_{0.95}}$ (Fig. 7B).

REFERENCES

1 K. Atherton, G. Newbold and J.A. Hockey, Discuss. Faraday Soc., 52 (1971) 33.
2 R.J. Kokes, Acc. Chem. Res., 6 (7) (1973) 266.
3 M. Nagao, M. Kiriki, H. Muraishi and T. Morimoto, J. Phys. Chem., 82 (24) (1978) 2561.
4 K. Mematsu, N. Ohkuma, N. Mizutani and M. Kato, J. Solid State Chem., 25 (2) (1978) 205.
5 G. Mattmann, H.R. Oswald and F. Schweizer, Helv. Chim. Acta, 55 (4), (1972) 1249.
6 M. Nagao, J. Phys. Chem., 75 (25) (1971) 3822.
7 S. Ishihara, N. Ohkuma, K. Mematsu, N. Mizutani and M. Kato, Nippon Kagaku Kaishi, 1 (1978) 60.
8 V.R. Choudhary, Ind. Eng. Chem., Prod. Res. Dev., 16 (1977) 12.
9 P.O. Scokart, S.A. Selim, J.P. Damon and P.G. Rouxhet, J. Colloid Interface Sci., 70 (1979) 209.
10 K. Tanabe, C. Ishiya, I. Matsuzaki, I. Ichikawa and H. Hattori, Bull. Chem. Soc. Jpn., 45 (1972) 47.
11 M. Itoh, H. Hatorri and K. Tanabe, J. Catal., 35 (1974) 225.
12 R.Sh. Mikhail, N.M. Guindy and I.I. Ali, J. Appl. Chem. Biotechnol., 26 (4) (1976) 199.
13 A. Amin, S. Hanafi and S.A. Selim, Thermochim. Acta, 53 (1982) 125.
14 K. Tanabe, M. Itoh, K. Morishige and H. Hattori, in B. Delmon, P.A. Jacobs and G. Poncelet, Preparation of Catalysts, Elsevier, Amsterdam, 1976.
15 Y. Fukuda, F. Fukushima, T. Matsuoka, T. Nitto and S. Hayokawa, Jpn. Kokai Tokkyo Koho, 78, 83, 996, 24 July (1978).
16 R.E. Semples and P.G. Rouxhet, J. Colloid Interface Sci., 55 (1976) 263.
P.G. Rouxhet and R.E. Sempels, J. Chem. Soc., Faraday Trans. 1, 70 (1974) 2021.
17 Powder Diffraction File, ASTM Alphabetical Index of Inorganic Compounds, International Center for Diffraction Data, PA, 19081, U.S.A. 1978.
18 K. Nakamoto (Ed.), 'Infrared Spectra of Inorganic and Coordination Compounds, John Wiley, New York and London, 1962.
19 M.R. Basila and T.R. Kantner, J. Phys. Chem., 71 (1967) 467.
20 T. Morimoto, H. Yanai and M. Nagao, J. Phys. Chem., 80 (1976) 471.
21 K. Tanabe, C. Ishiya, I. Matsuzaki, I. Ichikawa and H. Hattori, 23rd Annual Meeting of the Japanese Chemical Society, 1970, No. 03408 (in Japanese).
22 S.G. Gregg and K.S.W. Sing, Adsorption, Surface Area and Porosity, Academic Press, London, 1967.
23 B.G. Linsen (Ed.), Physical and Chemical Aspects of Adsorbents and Catalysts, Academic Press, New York, 1970.

24 S.A. Selim and S. Hanafi, Surf. Technol., 12 (1981) 287.
25 B.C. Lippens, B.G. Linsen and J.H. De Boer, J. Catal., 3 (1964) 32.
J.H. De Boer, B.G. Linsen and Th.J. Osinga, J. Catal., 4 (1965) 643.
26 R.Sh. Mikhail, M.M. Guindy and S. Hanafi, Egypt. J. Chem., Special Issue Tourky (1973) 53.
27 J.D. Carruthers, P.A. Cutting, R.E. Day, M.R. Harris, S.A. Mitchell and K.S.W. Sing, Chem. Ind., (1968) 1772.
28 R.Sh. Mikhail and F. Shebl, J. Colloid Interface Sci., 34 (1) (1970) 65.
29 S. Hanafi, S.A. Selim, A. Amin and P.G. Rouxhet, Surf. Technol., 13 (1981) 265.